UNIVERSIDADE SÃO PAULO
[1]INSTITUTO DE FÍSICA DE SÃO CARLOS
[2] INSTITUTO DE FÍSICA

Author: Yuri Peres Asnis[1]

MAGNETIC ISLAND BIFURCATION IN A VISCO-RESISTIVE MHD FLUID

Course completion assignment project presented to the Undergraduate Program at the São Carlos Institute of Physics, University of São Paulo, to the degree of Bachelor of Physics, Major in Theoretical and Experimental.

Advisor: Prof. Dr. Gustavo Paganini Canal[2]

São Carlos, 2020

Asnis, Yuri Peres

Magnetic Island Bifurcation in a visco-resistive MHD fluid / Yuri Peres Asnis; advisor Gustavo Paganini Canal - São Carlos, 2020.

24p.

Course completion assignment (Bachelor of Physics) - São Carlos Institute of Physics, University of São Paulo, 2020.

1.Island bifurcation. 2. Edge localized modes. 3. Resonant magnetic perturbations. 4. Magnetohydrodynamic. I. Canal, Gustavo Paganini, advisor.

Abstract

This work seeks to provide an improved understanding about the mechanisms responsible for a new class of magnetic topology bifurcations observed when an externally applied, small, non-axisymmetric, resonant magnetic perturbations (RMPs) that are used to suppress instabilities known as edge localized modes, which appear in the edge of tokamak plasmas. One possible mechanism for the observed bifurcations is the interaction between magnetohydrodynamic (MHD) modes located in different magnetic surfaces. Here, this mechanism is studied through a toy model that can describe such an interaction. Firstly, an analytical model was developed using a set of ideal MHD equations to describe the effect of a $m/n = 2/1$ kink (non-resonant) mode on the $q = 3$ surface, where the bifurcation is expected to occur. In this model, the externally applied RMP field is included self-consistently to account for the plasma response to such perturbations. Calculations of Poincaré sections shows that the toy model is capable of creating a $m/n = 2/1$ non-resonant mode that causes a kink in the magnetic field lines across the $q = 3$ surface. To see if such a kink is helping the island to bifurcate, a set of visco-resistive MHD equations needs to be used to model the resonant modes. The ultimate goal of this work is to provide a better insight into the physics basis responsible for the island bifurcations observed in the M3D-C1 simulations.

Keywords: Island bifurcation. Edge localized modes. Resonant magnetic perturbations. Magnetohydrodynamic.

Contents

1 Introduction

Access to energy is a key pillar for human wellbeing and ensuring that everyone has sufficient access to it became a challenge for global development. However, our energy consumption is having a significant negative impact on environment as the current energy demand is almost totally supplied by fossil fuels, whose burn releases carbon dioxide, among other greenhouse gases, which are the fundamental driver for global climate change (1), Figure 1. The problem becomes worst as the demand for energy is growing due to economic growth of developing countries and also due to an increase of their populations.

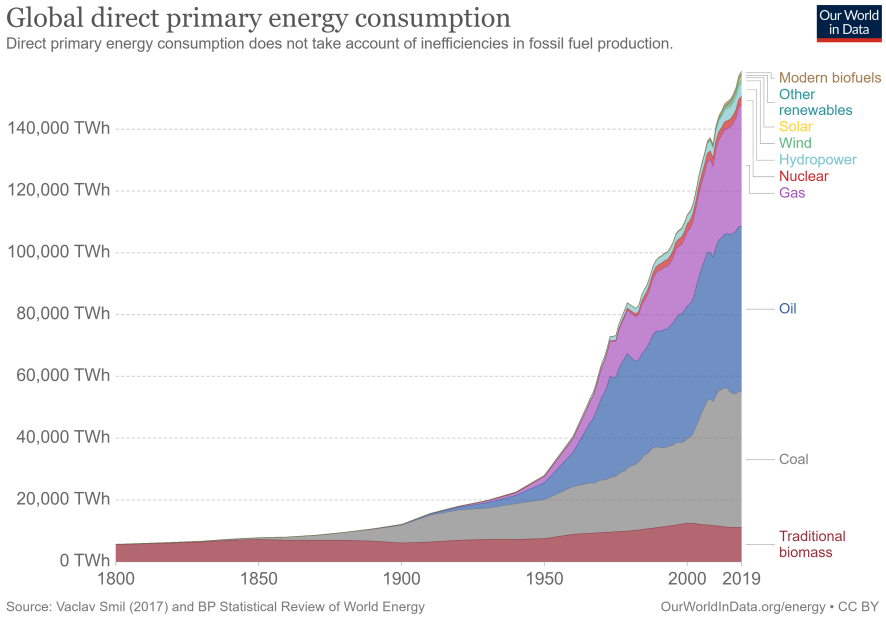

Figure 1: Global energy consumption separated by energy resource.
Source: RITCHIE (1).

Growing energy consumption makes the challenge of transitioning our energetic matrix away from fossil fuels towards low-carbon energy sources more difficult - new low-carbon energy has to meet this additional demand and try to displace existing fossil fuels in the energy mix. Nowaday, there are very few realistic scenarios in which fossil fuels are completelly replaced by other energy resorces and, in the absence of a solution, alternatives must be researched and developed. Nuclear fusion is considered a promising and possible long-term solution for the world's energy problem due to its potential to provide a clean and renewable energy (2).

1.1 Controlled Thermonuclear Fusion

Nuclear fusion is the process whereby two light nuclei fuse to form a heavier one, with the total final mass being slightly lower than the total initial mass. The mass difference (Δm) appears as energy according to Einstein's law, $E = \Delta mc^2$. Usually, these two light nuclei are hydrogen isotopes and the main reactions are

$$\begin{aligned} {}^2D + {}^2D &= {}^3H_e + {}^1n + 3.27 \text{ MeV}, \\ {}^2D + {}^2D &= {}^3H_e + {}^1H + 4.03 \text{ MeV}, \\ {}^2D + {}^3T &= {}^4H_e + {}^1n + 17.58 \text{ MeV}, \\ {}^2D + {}^3T &= {}^4H_e + {}^1H + 18.34 \text{ MeV}, \end{aligned} \tag{1}$$

where ${}^1H$, ${}^2D$, ${}^3T$, ${}^{3,4}H_e$ and ${}^1n$ represents hydrogen, deuterium, tritium, helium isotopes and neutron, respectively. The basic problem in achieving controlled fusion is to generate a plasma at very high temperatures (around 10 *keV*) and hold its constituents together long enough for a substantial number of fusion reactions to take place (3).

Fusion fuels are widely available and nearly inexhaustible. Deuterium can be distilled from all forms of water, while tritium will be produced inside the reactor as fusion-born neutrons react with lithium located in the surrounds of the reactor. Terrestrial reserves of lithium would permit the operation of fusion power plants for more than 1000 years, while sea-based reserves of lithium would fulfil needs for millions of years. Fusing atoms together in a controlled way releases nearly four million times more energy than a chemical reaction such as the burning of coal, oil or gas, and about seven times more than nuclear fission reactions. Nuclear fusion has, therefore, the potential of providing the kind of base-load energy supply needed to provide electricity to cities and industries. Additionally, nuclear fusion has the advantage of not emitting harmful toxins like carbon dioxide or other greenhouse gases into the atmosphere. Its major by-product is helium: an inert and non-toxic gas.

1.2 The tokamak concept

Invented by Soviet physicists Igor Tamm and Andrei Sakharov in the 1950s, the tokamak concept was created to confine thermonuclear plasmas and has become the most developed magnetic fusion concept. A tokamak is composed by a toroidal vacuum chamber with magnetic coils,

Figure 2. One of these coils is the central solenoid is responsible for producing the plasma current, which creates the poloidal magnetic field. In addition, toroidal and poloidal sets of coils are responsible for producing the toroidal magnetic field, and for both positioning and shaping of the plasma, respectively (4).

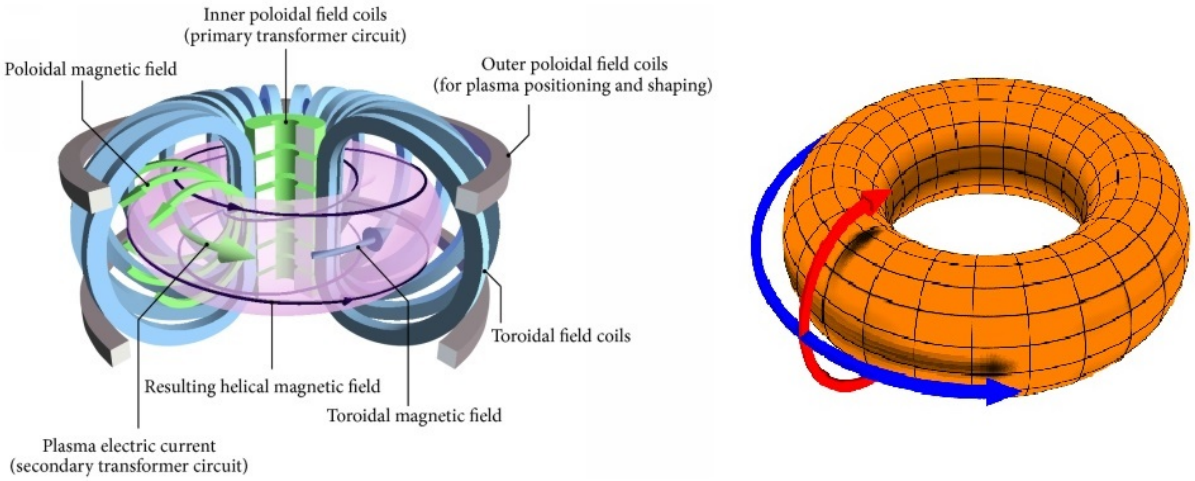

Figure 2: Left: Schematic of a tokamak. (b) Diagram depicting the poloidal (θ) direction, represented by the red arrow, and the toroidal (ϕ) direction, represented by the blue arrow. The major radius, R_0, is measured from the center of the machine while the minor radius, a, is the plasma horizontal radius.

Source: EUROFUSION (5)

In tokamaks, the twist of the magnetic field lines in each flux surface is parameterized by the so-called safety factor

$$q = \frac{\partial \Phi}{\partial \psi}, \tag{2}$$

where ψ is the poloidal magnetic flux and Φ the toroidal magnetic flux. The value of q on a flux surface corresponds to the number of toroidal turns a field line needs to complete in order to complete one turn in the poloidal direction. When $q = m/n$, where m and n are integers, the magnetic field lines close upon themselves after m toroidal turns and n poloidal turns. The use of the word "safety" when referring to the quantity q is directly related to the stability of plasmas (6).

1.3 MHD equilibrium and stability

Magnetohydrodynamics (MHD) is a physical-mathematical framework that concerns about the dynamics of magnetic fields in electrically conduction fluids and it is the most widely used model to predict tokamak plasma instabilities. The fundamental concept behind MHD is that magnetic fields can induce currents in moving conductive fluids, which in turn change the original magnetic field. From the earliest experiments, it was clear that tokamak plasmas are subject to a variety of macroscopic instabilities. Although many of these instabilities are not fully understood, they can be attributed to identifiable MHD modes. In the frame of resistive MHD, i.e. in plasmas that cannot be treated as a perfect conductor, instabilities driven by the radial gradient of the equilibrium toroidal plasma current can develop (7). The consideration of the plasma resistivity removes constrains that are present in the ideal MHD model, making states of lower magnetic energy now accessible to the plasma. When resistive MHD instabilities occur, they usually cause a change in the magnetic topology. In particular, resistivity allows magnetic field lines to break and reconnect, causing other classes of instabilities to occur such as tearing modes. The name of these modes derives from the tearing and rejoining of the magnetic field lines that occur during the instability as a consequence of the finite resistivity. Reconnection of magnetic field lines in tokamak plasmas occurs at resonant surface, and leads to the formation of structures named magnetic islands, Figure 3. In practice, the formation of magnetic islands will always occur to some extent in the non-linear evolution of any MHD instability.

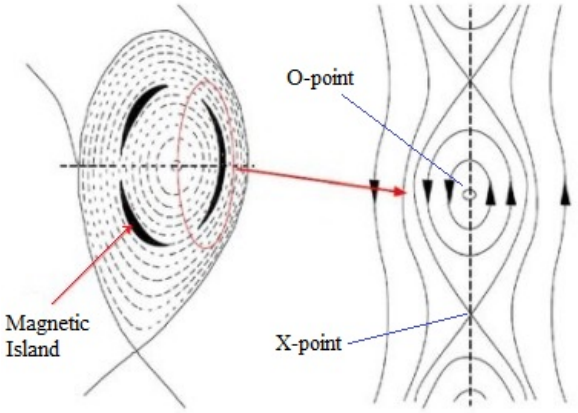

Figure 3: A magnetic island in a toroidally-shaped plasma and its elliptic fixed-point (O-point) and hyperbolic fixed-points (X-point).
Source: Adapted from SICCINIO (8)

1.4 The triggering of ELMs and the need for ELM control coils

In 1982 a new confinement regime was discovered in the ASDEX tokamak by Friedrich Wagner and co-workers. This new confinement mode, known as high confinement mode (H-mode), is characterized by a confinement time 2 to 3 times longer than in the low confinement mode (L-mode) (9). The most important feature of the H-mode is the formation of a transport barrier at the plasma edge leading to pedestals in the density and temperature profiles (10). However, plasmas in the H-mode are found to be unstable to instabilities termed as Edge Localized Modes (ELMs), which are ideal MHD modes driven by plasma pressure gradient and parallel current density in the plasma edge. The crash of these modes releases a significant fraction of the plasma thermal energy into the plasma scrape-off layer and that can lead to unacceptably high transient heat fluxes onto the divertor targets (11). The erosion caused by these bursts of energy can reduce significantly the lifetime of the plasma-facing components thus driving the need for ELM control.

Several experimental, numerical and theoretical studies worldwide have demonstrated that the presence of relatively small, non-axisymmetric, resonant magnetic perturbations (RMP), created by currents flowing in non-axisymmetric coils outside the plasma, can be used to suppress ELMs (12). The first experimental demonstration of ELM suppression was carried out in the DIII-D tokamak during the 2003 campaign, and since than, there has been a rapid worldwide growth in theoretical, numerical and experimental edge RMP research, which resulted in the addition of ELM control coils to the International Thermonuclear Experimental Reactor (ITER) baseline design (13), Figure 4.

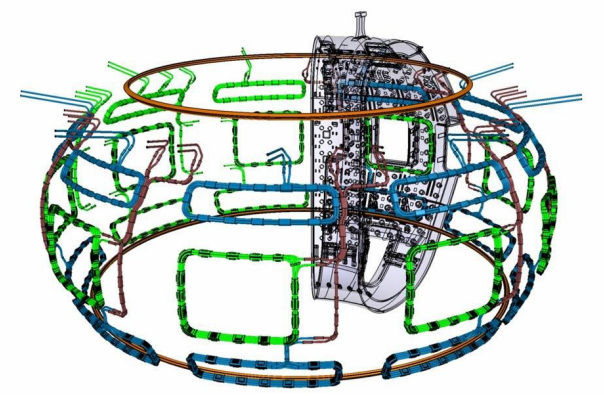

Figure 4: The ITER RMP coils for ELM control in green and blue.
Source: ITER Website (13)

2 Motivation

Resistive MHD theory and simulations are fundamental tools for understanding the physics of topological bifurcations in the trajectories of magnetic field lines that are attributed to tearing and reconnection in magnetically confined toroidal plasmas. While magnetic field line reconnection theory is conceptually well established and widely accepted, there are open questions concerning the detailed dynamics responsible for these topological changes that are not yet fully understood (14). In resonantly perturbed plasmas, theory predicts that only three parameters are required to determine the topology of a fully reconnected magnetic state, namely the normalized plasma viscosity, rotation, and resistivity (15).

Recent calculations of linear plasma responses to $n = 3$ RMP fields, using the resistive MHD code M3D-C1 (16), revealed a new class of magnetic field line topology bifurcations that do not fit into the three-parameter bifurcation theory (17, 18). Figure 5(a) shows a magnetic island at the q = 3 surface of a plasma created in the National Spherical Torus eXperiment Upgrade (NSTX-U) (19), created by an RMP current $I_{RMP} = 1$ kA. An increase in I_{RMP} causes a dramatic change in the topological structure of the flux surfaces inside of the island. As I_{RMP} increases, the island width increases and its O-point moves to the right while a sub-set of flux surfaces inside of the island stretch asymmetrically in the opposite direction. Note that the position of the X-points remains constant during this process. As shown in the $I_{RMP} = 4$ kA panel, the elongated lobe has bifurcated to form a new set of MHD island elliptic and hyperbolic fixed-points inside the original island. Note that this bifurcation occurs again at $I_{RMP} = 16$ kA.

These results not only challenge forced resonant tearing and reconnection theory of tokamak plasmas, with relatively high plasma pressures, but are particularly important for understanding the underlying physics of self-organization in toroidal plasmas. The topology of the magnetic equilibrium field in toroidal plasmas plays an essential role in determining the properties of the energy, particle and momentum confinement, as well as in its MHD stability. Understanding the mechanisms responsible for this new class of topological bifurcations is, therefore, of particular importance in self-sustained burning or ignited states as the ability of the plasma to self-organize can open access to new types of operating regimes with improved confinement.

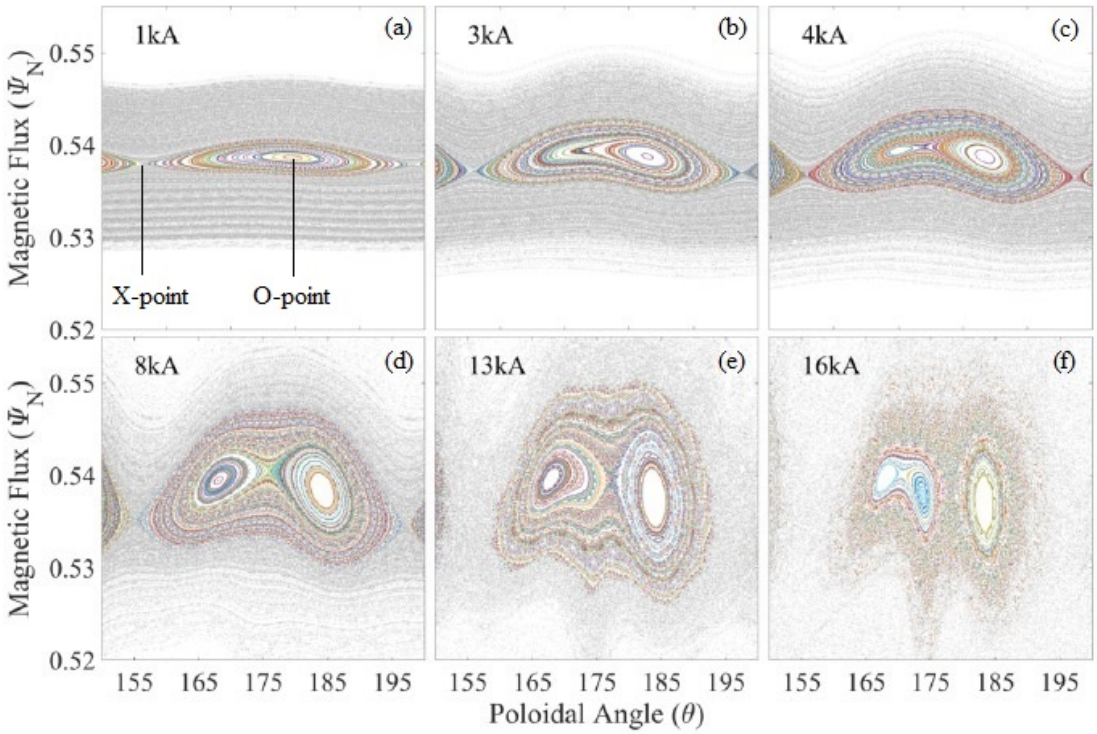

Figure 5: Poincaré section showing topological changes in the flux surfaces inside of the magnetic island in a NSTX-U equilibrium at $q = 3$ as I_{RMP} is increased from 1 kA to 16 kA.
Source: Adapted from EVANS, T. E. *et al.* (17)

3 Methodology

The goal of this project is to identify the specific features a rotating plasma equilibrium needs in order for an externally applied RMP field to cause an heteroclinic magnetic island bifurcation. In order to understand it, the MHD equations are linearized around a generic rotating plasma equilibrium and a static n = 1 RMP field is applied to the plasma. The plasma will respond to this external magnetic field with perturbations in all the plasma equilibrium parameters. This set of perturbations is referred to as the plasma response. With the equilibrium magnetic field, the RMP field, and the perturbed field due to by the plasma response, a code was developed to follow the magnetic field lines in order to generate Poincaré sections, such as the one shown in Figure 5, which will be used to search for heteroclinic island bifurcations.

A Poincaré section consists of a surface in the phase-space transversal to the flow of the system that intersects orbits of interest. Each intersection in the section may be considered as an initial condition, and if the system is bounded, one can expect the orbit to return and cross again the surface.

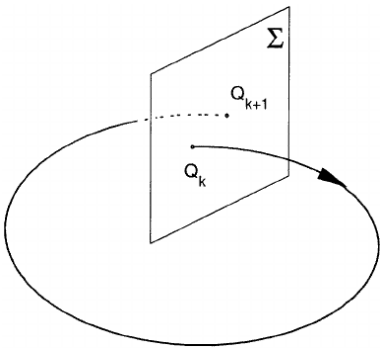

Figure 6: Scheme of a Poincaré section Σ where Q_k is the orbit which intersects the surface. Source: ABDULLAEV, S. S. (21)

4 Results

4.1 The MHD toy model

Within the MHD framework, the main quantities that characterize the state of the electrically conducting fluid are the plasma mass density, ρ_m, plasma velocity, $\boldsymbol{u}$, plasma pressure, p, electric field, $\boldsymbol{E}$, magnetic field, $\boldsymbol{B}$, and electric current density, $\boldsymbol{J}$. In near-Maxwellian plasmas without pressure anisotropy, the single-fluid visco-resistive MHD equations in their simplest form are,

$$\frac{\mathscr{D}\rho_m}{\mathscr{D}t} = -\rho_m\,(\boldsymbol{\nabla}\cdot\boldsymbol{u}) \qquad \text{(Continuity Equation)}, \tag{3}$$

$$\frac{\mathscr{D}p}{\mathscr{D}t} = -\Gamma p\,(\boldsymbol{\nabla}\cdot\boldsymbol{u}) \qquad \text{(Energy Equation)}, \tag{4}$$

$$\rho_m\frac{\mathscr{D}\boldsymbol{u}}{\mathscr{D}t} = \boldsymbol{J}\times\boldsymbol{B} - \boldsymbol{\nabla}p + \mu\rho_m\left[\nabla^2\boldsymbol{u} + \frac{1}{3}\boldsymbol{\nabla}\,(\boldsymbol{\nabla}\cdot\boldsymbol{u})\right] \qquad \text{(Momentum Equation)}, \tag{5}$$

$$\frac{\partial\boldsymbol{B}}{\partial t} = -\boldsymbol{\nabla}\times\boldsymbol{E} \qquad \text{(Faraday's Law)}, \tag{6}$$

$$\mu_0 \boldsymbol{J} = \boldsymbol{\nabla} \times \boldsymbol{B} \qquad \text{(Ampère's Law)}, \tag{7}$$

$$\eta \boldsymbol{J} = \boldsymbol{E} + \boldsymbol{u} \times \boldsymbol{B} \qquad \text{(Ohm's Law)}, \tag{8}$$

with μ_0 being the vacuum magnetic permeability, η the plasma electric resistivity, μ the kinematic viscosity, $\Gamma = 5/3$ the ratio of specific heats, and $\frac{\mathscr{D}}{\mathscr{D}t} = \frac{\partial}{\partial t} + \boldsymbol{u} \cdot \boldsymbol{\nabla}$ is the convective derivative. In order to reduce the number of equations, one can combine Maxwell's equations with Ohm's Law and the conservation of momentum equation.

Combined Maxwell-Ohm's Law

The replacement of $\boldsymbol{J}$ from Ampère's Law into Ohm's Law yields

$$\frac{\eta}{\mu_0} \boldsymbol{\nabla} \times \boldsymbol{B} = \boldsymbol{E} + \boldsymbol{u} \times \boldsymbol{B}. \tag{9}$$

Taking the curl of the equation above, considering that the resistivity is spatially constant, and using Faraday's Law, yields

$$\frac{\eta}{\mu_0} \nabla^2 \boldsymbol{B} + \boldsymbol{\nabla} \times (\boldsymbol{u} \times \boldsymbol{B}) = \frac{\partial \boldsymbol{B}}{\partial t}. \tag{10}$$

Here, the vectorial identity $\left[\boldsymbol{\nabla} \times (\boldsymbol{\nabla} \times \boldsymbol{B}) = \boldsymbol{\nabla} (\boldsymbol{\nabla} \cdot \boldsymbol{B}) - \nabla^2 \boldsymbol{B}\right]$ was used while calculating the curl of the left-hand side of Eq. (9).

Combined Momentum-Ampère Law

Replacing $\boldsymbol{J}$ from Ampère's Law into the Momentum conservation equation yields

$$\rho_m \frac{\mathscr{D}\boldsymbol{u}}{\mathscr{D}t} = \frac{1}{\mu_0} (\boldsymbol{B} \cdot \boldsymbol{\nabla}) \boldsymbol{B} - \boldsymbol{\nabla} \left(p + \frac{B^2}{2\mu_0} \right) + \mu \rho_m \left[\nabla^2 \boldsymbol{u} + \frac{1}{3} \boldsymbol{\nabla} (\boldsymbol{\nabla} \cdot \boldsymbol{u}) \right]. \tag{11}$$

Here the vectorial identity $\left[\boldsymbol{B} \times (\boldsymbol{\nabla} \times \boldsymbol{B}) = (\boldsymbol{B} \cdot \boldsymbol{\nabla}) \boldsymbol{B} - \frac{1}{2} \boldsymbol{\nabla} (\boldsymbol{B} \cdot \boldsymbol{B})\right]$ was used.

4.2 The equilibrium equations

The proposal of using a simplified model to calculate the stationary response of plasmas to RMP fields requires the description of non-axysimmetric MHD equilibria, which are obtained by setting the time derivatives to zero in equations (3), (4), (10) and (11). Consequently, the subset of steady-state MHD equations are

$$\rho_m \boldsymbol{\nabla}\cdot\boldsymbol{u} + \boldsymbol{u}\cdot\boldsymbol{\nabla}\rho_m = 0, \tag{12}$$

$$\Gamma p \boldsymbol{\nabla}\cdot\boldsymbol{u} + \boldsymbol{u}\cdot\boldsymbol{\nabla} p = 0, \tag{13}$$

$$\frac{\eta}{\mu_0}\nabla^2\boldsymbol{B} + \boldsymbol{\nabla}\times\big(\boldsymbol{u}\times\boldsymbol{B}\big) = 0, \tag{14}$$

$$\rho_m\big(\boldsymbol{u}\cdot\boldsymbol{\nabla}\big)\boldsymbol{u} = \frac{1}{\mu_0}\big(\boldsymbol{B}\cdot\boldsymbol{\nabla}\big)\boldsymbol{B} - \boldsymbol{\nabla}\left(p + \frac{B^2}{2\mu_0}\right) + \mu\rho_m\left[\nabla^2\boldsymbol{u} + \frac{1}{3}\boldsymbol{\nabla}\big(\boldsymbol{\nabla}\cdot\boldsymbol{u}\big)\right]. \tag{15}$$

To solve this set of equations, a cylindrical coordinate system $\big(r,\theta,\phi\big)$ will be used to avoid the coupling of satellite modes (see Appendix A of (20) for details). Here, the z-coordinate was changed to $\phi = z/R_0$ to make a connection with the toroidal angle of a torus of major radius R_0 and minor radius a. Let's assume that the plasma has a purely axial equilibrium flow of the form $\boldsymbol{u_0}(r) = R_0\Omega_{0\phi}(r)\hat{\boldsymbol{e}}_{\boldsymbol{\phi}}$ and the equilibrium magnetic field is of the form $\boldsymbol{B_0}(r) = B_{0\theta}(r)\hat{\boldsymbol{e}}_{\boldsymbol{\theta}} + B_{0\phi}\hat{\boldsymbol{e}}_{\boldsymbol{\phi}}$. With these assumptions and assuming that there are non resistivity and non viscosity, the ideal MHD equilibria must obey

$$\boldsymbol{u_0}\cdot\boldsymbol{\nabla}\rho_{\mathrm{m0}} = 0, \tag{16}$$

$$\boldsymbol{u_0}\cdot\boldsymbol{\nabla} p_0 = 0, \tag{17}$$

$$\boldsymbol{\nabla}\times\big(\boldsymbol{u_0}\times\boldsymbol{B_0}\big) = 0, \tag{18}$$

$$\frac{1}{\mu_0}\big(\boldsymbol{B_0}\cdot\boldsymbol{\nabla}\big)\boldsymbol{B_0} = \boldsymbol{\nabla}\left(p_0 + \frac{B_0^2}{2\mu_0}\right). \tag{19}$$

Note that equations (16) and (17) imposes that both the equilibrium plasma density and pressure gradients must be perpendicular to the equilibrium plasma flow. These equations are automatically satisfied as both $\rho_{m0}(r)$ and $p_0(r)$, as any other equilibrium quantity, depends only on the radial coordinate, i.e. $\boldsymbol{\nabla}\rho_{m0}$ and $\boldsymbol{\nabla} p_0$ point in the radial direction. In addition, all the equilibrium plasma parameters depends only on the radial coordinates. Their exact profiles and specific

parameters are

$$B_{0\phi}(r) = B_{o\phi}, \tag{20}$$

$$\Omega_{0\phi}(r) = \hat{\Omega}_{0\phi}\left[1-\left(\frac{r}{a}\right)^2\right]^{\alpha}, \tag{21}$$

$$\rho_{m0}(r) = \hat{\rho}_{m0}\left[1-\left(\frac{r}{a}\right)^2\right]^{\gamma}, \tag{22}$$

$$B_{0\theta}(r) = \frac{\mu_0 I_P}{2\pi r}\left\{1-\left[1-\left(\frac{r}{a}\right)^2\right]^{\nu+1}\right\}, \tag{23}$$

$$p_0(r) = \int_a^r \left[\frac{1}{\mu_0}\left(\boldsymbol{B_0}\cdot\boldsymbol{\nabla}\right)\boldsymbol{B_0} - \boldsymbol{\nabla}\left(\frac{B_0^2}{2\mu_0}\right)\right] dr'. \tag{24}$$

With these forms for the equilibrium profiles and the parameters given in Table 1, the equilibrium plasma quantities can be calculated, Figure 7.

Table 1: Equilibrium parameters used in this work.

Equilibrium parameters		
Tokamak	$a = 0.2$m	$R_0 = 0.6$m
Poloidal field	$I_p = 100$ kA	$\nu = 7$
Toroidal field	$B_{0\phi} = 1.5$ T	constant
Rotation	$\hat{\Omega}_{0\phi} = 69.2$ krad/s	$\alpha = 2$
Mass density	$\hat{\rho}_{m0} = 1.55\times10^{20}$ m^{-3}	$\gamma = 0.2$

Source: By the author.

One result that can be inferred from the equilibrium parameters is the safety factor. In cylindrical coordinates the safety factor can be written as $q = \frac{rB_{0\phi}}{R_0 B_{0\theta}}$ and, therefore, one can understand why it is possible to work with the ideal MHD equations once the goal is to observe the impact of the $m/n = 2/1$ mode at $q = 3$ flux surface. The resistivity will play a role only in the vicinity of the $q = 3$, and since the applied RMP field is non-resonant at this surface, resistivity can be neglected in the equations. The q-profile obtained using the equilibrium quantities given by Equations 20 to 24 can be seen in Figure 8.

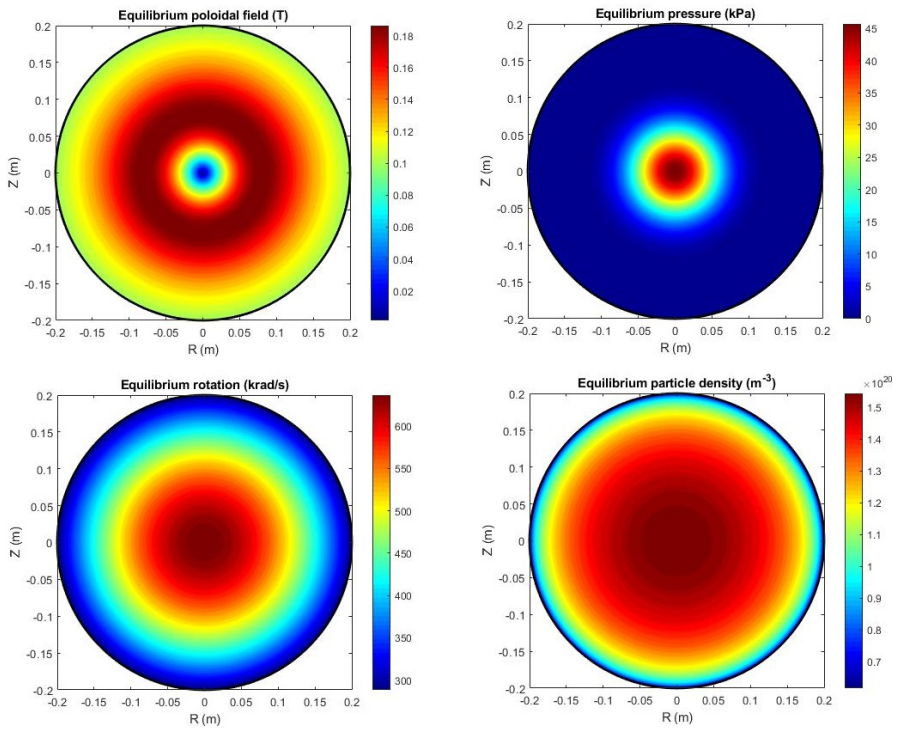

Figure 7: Plasma quantities across de plasma cross section: From left to right: poloidal field, plasma pressure, plasma toroidal rotation and plasma density, respectively.
Source: By the author

4.3 Linearized MHD equations

In this section, the subset of Equations (12) to (15) are linearized around an axisymmetric equilibrium, where all the plasma parameters will be expanded in Fourier series:

$$\text{Scalar quantities}: f(r,\theta,\phi) = f_0(r) + \sum_{m,n=-\infty}^{\infty} f_1^{m,n}(r) e^{i(m\theta - n\phi)} \tag{25}$$

$$\text{Vectorial quantities}: \boldsymbol{A}(r,\theta,\phi) = \boldsymbol{A_0}(r) + \sum_{m,n=-\infty}^{\infty} \boldsymbol{A_1^{m,n}}(r) e^{i(m\theta - n\phi)} \tag{26}$$

$$\text{Magnetic field}: \boldsymbol{B}(r,\theta,\phi) = \boldsymbol{B_0}(r) + \sum_{m,n=-\infty}^{\infty} \left[\boldsymbol{B_{1,vac}^{m,n}}(r) + \boldsymbol{B_{1,resp}^{m,n}}(r) \right] e^{i(m\theta - n\phi)} \tag{27}$$

Here, $\boldsymbol{B_{1,vac}^{m,n}}(r)$ is the RMP field necessary to suppress the ELMs and $\boldsymbol{B_{1,resp}^{m,n}}(r)$ is the plasma response. Also, $f_1^{m,n}(r) \ll f_0(r)$ and $|\boldsymbol{A_1^{m,n}}(r)| \ll |\boldsymbol{A_0}(r)|$, which means one can neglect perturbed

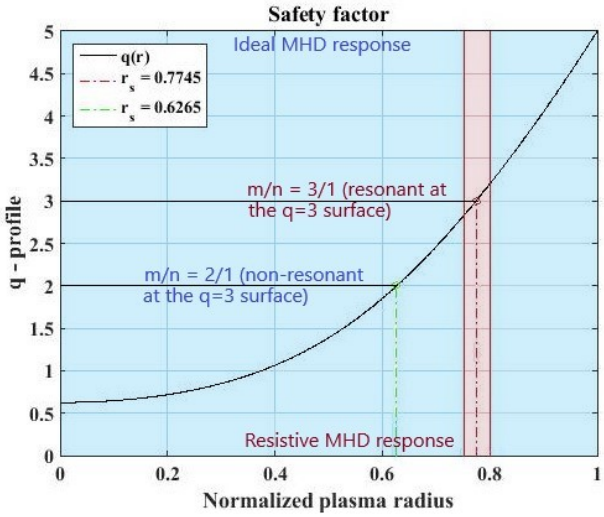

Figure 8: q-profile as a function of normalized plasma radius. Green and red vertical dashed lines indicate the location of the $q = 2$ and $q = 3$ surfaces.
Source: By the author

terms of second-order or higher.

The magnetic field lines around the $q = 3$ surface will be affected by a resonant $m/n = 3/1$ tearing mode and also by a $m/n = 2/1$ kink mode at the $q = 2$ surface, which extends up to the q = 3 surface. The calculation of the plasma response due to the resonant (tearing) mode requires the use of resistive MHD Equations (12) to (15). However, there is no need to solve the resistive layer for the non-resonant m/n = 2/1 mode. This mean ideal MHD can be used instead, i.e. neglecting resistive and viscous terms, to solve the plasma response due to the $m/n = 2/1$ mode. Applying the linearization procedure described above to the steady-state MHD Equations (12) to (15) and using the equilibrium relations (16) and (19) yields

$$\boldsymbol{u_0}\cdot\boldsymbol{\nabla}\rho_{m1}+\boldsymbol{u_1}\cdot\boldsymbol{\nabla}\rho_{m0}+\rho_{m0}\boldsymbol{\nabla}\cdot\boldsymbol{u_1}=0, \tag{28}$$

$$\boldsymbol{u_0}\cdot\boldsymbol{\nabla}p_1+\boldsymbol{u_1}\cdot\boldsymbol{\nabla}p_0+\Gamma p_0\boldsymbol{\nabla}\cdot\boldsymbol{u_1}=0, \tag{29}$$

$$\frac{\eta}{\mu_0}\nabla^2\boldsymbol{B_1}+\boldsymbol{\nabla}\times\left(\boldsymbol{u_1}\times\boldsymbol{B_0}+\boldsymbol{u_0}\times\boldsymbol{B_1}\right)=0, \tag{30}$$

$$\rho_{m0}\left[\left(\boldsymbol{u_0}\cdot\boldsymbol{\nabla}\right)\boldsymbol{u_1}+\left(\boldsymbol{u_1}\cdot\boldsymbol{\nabla}\right)\boldsymbol{u_0}\right]=\frac{1}{\mu_0}\left[\left(\boldsymbol{B_1}\cdot\boldsymbol{\nabla}\right)\boldsymbol{B_0}+\left(\boldsymbol{B_0}\cdot\boldsymbol{\nabla}\right)\boldsymbol{B_1}\right]- \tag{31}$$

$$-\boldsymbol{\nabla}\left(p_1+\frac{\boldsymbol{B_0}\cdot\boldsymbol{B_1}}{\mu_0}\right)+\mu\rho_{m0}\left[\nabla^2\boldsymbol{u_1}+\frac{1}{3}\boldsymbol{\nabla}\left(\boldsymbol{\nabla}\cdot\boldsymbol{u_1}\right)\right]. \tag{32}$$

4.4 The plasma response

By obtaining the linearized MHD Equations (29) to (32) around the axisymmetric equilibrium, one end up with eight equations and eight unknowns. After an extensive algebra, all the plasma parameters can be written in terms of $B_{1r}=B_{1r}^{vac}+B_{1r}^{resp}$ in the form

$$p_1=c_1(r)B_{1r}, \tag{33}$$

$$\rho_{m1}=c_2(r)B_{1r}, \tag{34}$$

$$u_{1r}=c_3(r)B_{1r}, \tag{35}$$

$$u_{1\theta}=c_4(r)B_{1r}+c_5(r)\frac{dB_{1r}}{dr}, \tag{36}$$

$$u_{1\phi}=c_6(r)B_{1r}+c_7(r)\frac{dB_{1r}}{dr}, \tag{37}$$

$$B_{1\theta}=c_8(r)B_{1r}+c_9(r)\frac{dB_{1r}}{dr}, \tag{38}$$

$$B_{1\phi}=c_{10}(r)B_{1r}+c_{11}(r)\frac{dB_{1r}}{dr}. \tag{39}$$

Where the c-functions depends only on equilibrium quantities. With these forms, the plasma response can be fully expressed by a second order differential equation (ODE) for B_{1r}^{resp}

$$\alpha_0(r)\frac{d^2B_{1r}^{resp}}{dr^2}+\beta_0(r)\frac{dB_{1r}^{resp}}{dr}+\gamma_0(r)B_{1r}^{resp}=S_0^{vac}(r), \tag{40}$$

where the source term $S_0^{vac}(r)$ depends only on equilibrium plasma quantities and the externally vacuum field B_{1r}^{vac}

$$S_0^{vac}(r) = -\alpha_0(r)\frac{d^2B_{1r}^{vac}}{dr^2} - \beta_0(r)\frac{dB_{1r}^{vac}}{dr} - \gamma_0(r)B_{1r}^{vac}. \tag{41}$$

Therefore, by solving the differential Equation 40, all the perturbed plasma parameters that define the plasma response will be fully determined.

4.4.1 Solving the second-order differential equation

The ODE variable coefficients $\alpha_0(r)$, $\beta_0(r)$ and $\gamma_0(r)$ can be easily calculated using the equilibrium plasma parameters exact forms. Therefore, using the built-in MATLAB numerical integrator ode45 it was possible to obtain the plasma response given the source term. With the radial

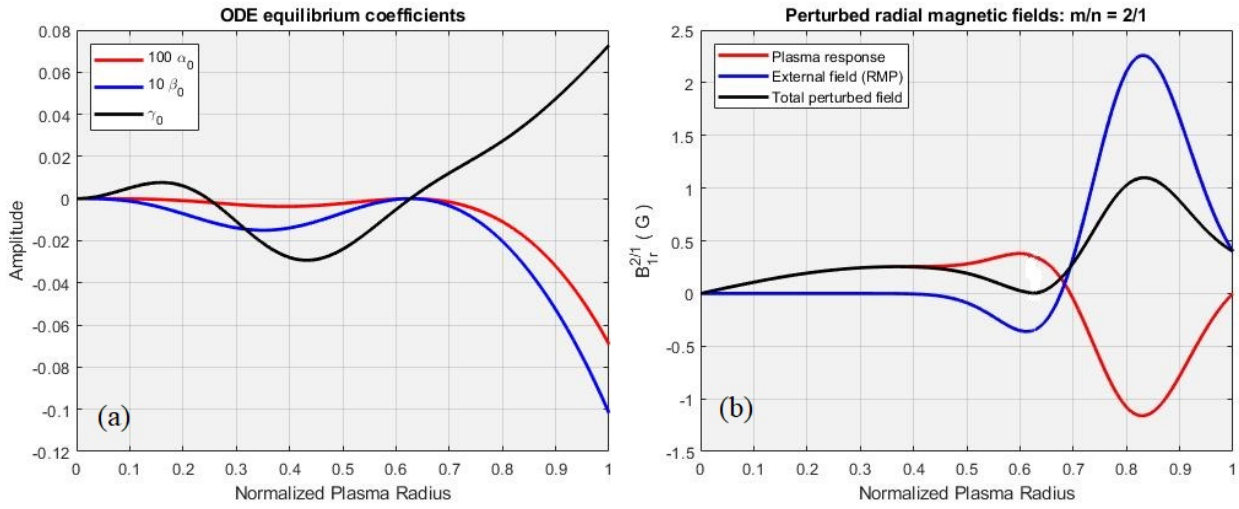

Figure 9: (a) ODE variables coefficients. (b) radial component of the perturbed magnetic field. Source: By the author

component of the total perturbed magnetic field obtained by solving the ODE, one can calculate the other two components of the perturbed magnetic field using the Equations (38) and (39).

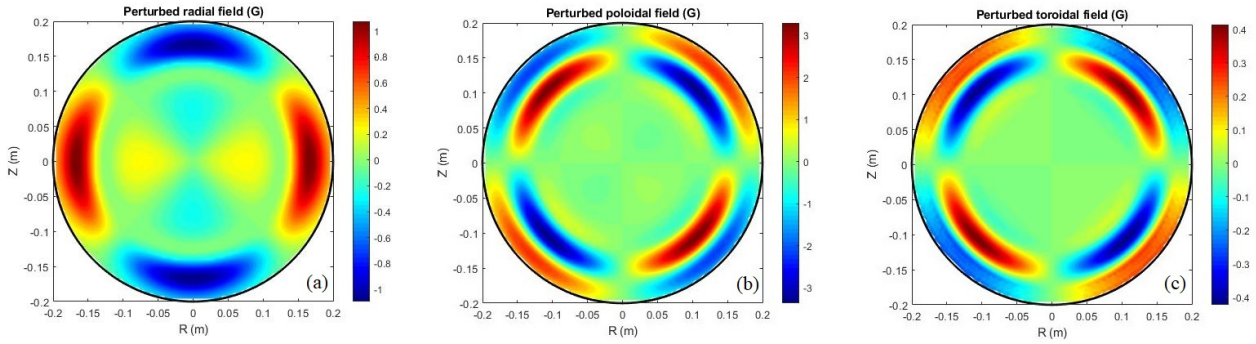

Figure 10: (a) Radial, (b) poloidal and (c) toroidal perturbed magnetic fields across the plasma cross section.

Source: By the author

4.4.2 Poincaré section

To understand the impact of the non-resonant $m/n = 2/1$ mode at the $q = 3$ flux surface, it is necessary to follow the magnetic field lines to generate Poincaré section. The procedure to create this section is to identify the differential equations that govern the field lines. The line differential in periodic cylindrical coordinates is

$$\left(dl_r, dl_\theta, dl_\phi\right) = \left(dr, r d\theta, R_0 d\phi\right) \tag{42}$$

By assuming that the line differential is always parallel to the magnetic field, one obtains the following relations

$$\frac{dr}{d\phi} = R_0 \frac{B_r}{B_\phi} = R_0 \frac{B_{0r} + B_{1r}}{B_{0\phi} + B_{1\phi}}, \tag{43}$$

$$\frac{d\theta}{d\phi} = \frac{R_0}{r} \frac{B_\theta}{B_\phi} = \frac{R_0}{r} \frac{B_{0\theta} + B_{1\theta}}{B_{0\phi} + B_{1\phi}}. \tag{44}$$

Where $B_{0r} = 0$, $B_{0\theta}$ and $B_{0\phi}$ are given in subsection 4.2, and the $\boldsymbol{B}_1$ components were just calculated. Here, one has used the Runge-Kutta 4th order method to solve both differential Equations (43) and (44) to obtain the Poincaré section for the total magnetic field.

Figure 11 shows a Poincaré section and, as it can be seen, the calculated non-resonant $m/n = 2/1$ kink mode is causing a kink in the magnetic surfaces around the $q = 3$ surface, which is located at the about $r/a = 0.7745$, the Figure 11. This is a satisfatory result because as the

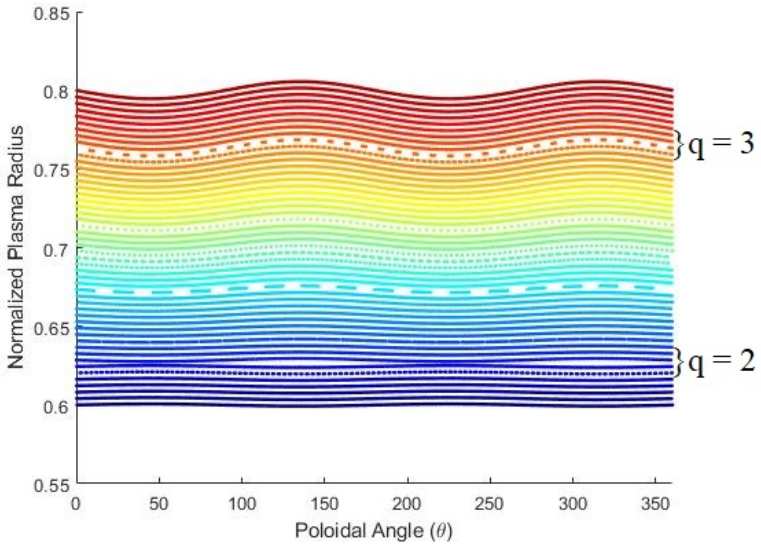

Figure 11: Poincaré section showing a kink in the magnetic field lines across the q = 3 surface.
Source: By the author

RMP current increases, the island width increases and twist as it is shown in Figure 5. Therefore, there is a kink mode present on the M3D-C1 simulations which could be helping the island to bifurcate.

5 Conclusion and outlook

The topology of the magnetic equilibrium field in toroidal plasmas plays an essential role in determining the properties of the energy, particle and momentum confinement, as well as in its MHD stability. Understanding the mechanisms responsible for this new class of topological bifurcations is, therefore, of particular importance in self-sustained burning or ignited states as the ability of the plasma to self-organize can open access to new types of operating regimes with improved confinement.

This work is the first step towards the development of an analytical model which might help to bring light on the origins of this bifurcation process. By solving the ideal MHD equations for the $m/n = 2/1$ mode it was possible to see that this mode is indeed causing a kink in the magnetic field lines around the $q = 3$ surface, which is located at 0.7745. This kink could be helping or even being the cause of the bifurcation of the magnetic island present in the $q = 3$ surface. Therefore, in order to answer what is causing the bifurcation, it is necessary to insert at least the resistivity back in the equations to create an island at the $q = 3$ flux surface and then apply the non-resonant $m/n = 2/1$ RMP field.

References

1. RITCHIE, H.. *Energy production and consumption*, 2019. Available from: https://ourworldindata.org/energy-production-consumption. Accessible at: March 04, 2021.

2. COWLEY, S.C. *The quest for fusion power*, 2016.Available from: https://www.nature.com/articles/nphys3719.Accessible at: March 04,2021.

3. BITTENCOURT, J. A.. *Fundamentals of plasma physics*. New York: Springer Verlag,2004.

4. ITER. *What is a tokamak*. Available from:https://www.iter.org/mach/Tokamak.Accessible at: March 02,2021.

5. EURO FUSION. *Figures*. Available from: https://http://figures.euro-fusion.org/Images/JG05.537-6c1500.1500.jpg. Accessible at: March 04, 2021.

6. FRIEDBERG, J. *Ideal magnetohydrodynamics*. New York: Plenum Press, 1987.

7. WESSON, J. A.. *Tokamaks*, 2nd. ed. Oxford: Clarendon Press, 1997.

8. SICCINIO, M.. *Kinetic investigation of magnetic islands in tokamaks*. Available from: `https://mediatum.ub.tum.de/doc/957027/957027.pdf`. 2010.

9. KEILHACKER, M.. H-mode confinement in tokamaks. *Plasma Physics and Controlled Fusion*, v.29, n.10,p.1401, 1987.

10. WAGNER, F. *et al*. Development of an edge transport barrier at the H-mode transition of ASDEX. *Physical Review Letters*,v. 53,p.453–1456, 1984.

11. LOARTE, A. *et al*. Characteristics of type I ELM energy and particle losses in existing devices and their extrapolation to ITER. *Plasma Physics and Controlled Fusion*, v.45, n.9, p.1549,2003.

12. EVANS,T.E. Resonant magnetic perturbations of edge-plasmas in toroidal confinement devices. *Plasma Physics and Controlled Fusion*, v.57, n.12,p.123001, 2015.

13. The ITER project. *International thermonuclear experimental reactor*.Available from: https://www.iter.org/.Accessible at: March,2021.

14. GONZALEZ, W. D. *et al*. Fundamental concepts associated with magnetic reconnection. *In*: GONZALEZ, W. D..;PARKER, E.(eds.) *Magnetic reconnection. astrophysics and space science library*. Switzerland: Springer International Publishing,2016.p.426.

15. FITZPATRICK, R.. Bifurcated states of a rotating tokamak plasma in the presence of a static error-field. *Physics of Plasmas*, v.5, p.3325,1998.

16. FERRARO, N. M. *et al*. Role of plasma response in displacements of the tokamak edge due to applied non-axisymmetric fields. *Nuclear Fusion*, v.53 n.7, p.073042, 2013.

17. EVANS, T. E. *et al*. *Observations of heteroclinic bifurcations in resistive mhd simulations ofthe plasma response to resonant magnetic perturbations*. 2018. Available from:https://arxiv.org/abs/1805.10394.Accessible at: March 2021.

18. BARDOCZI, L.; EVANS, T. E.. Discovery of magnetic island heteroclinic bifurcation in tokamaks.To appear in: *Physical Review Letters*, 2020.

19. MENARD, J. E. *et al*. Overview of the physics and engineering design of NSTX upgrade. *Nuclear Fusion*, v.52, n.8,p.083015, 2012.

20. CONNOR, J. W. *et al*. Resonant magnetohydrodynamic modes with toroidal coupling. part i:Tearing modes. *Physics of Fluids*, v.3,n.7,p.1532, 1991.

21. ABDULLAEV, S. S. A new integration method of Hamiltonian systems by sympletic maps. *Journal of Physics A*: general physics,v.32, n.15,p.2745-2766,1999.